Inversion Rise Model Based on Penetrative Convection[1]

ROLAND B. STULL

Dept. of Atmospheric Sciences, University of Washington, Seattle 98195

(Manuscript received 18 January 1973, in revised form 8 May 1973)

ABSTRACT

A mathematical model to describe the height changes and other characteristics of an inversion base under the influence of surface convection and general subsidence is developed. Inversion interface dynamics and entrainment rates are formulated based on an unstable boundary layer environment of well-organized, plume-like, penetrative convection. The use of unstable boundary layer scaling velocities in describing the convection leads to a natural inclusion of the relevant parameters associated with inversions into this model. It is found that the model does accurately predict realistic rates of inversion rise and of temperature changes for conditions where organized free convection is prevalent.

1. Introduction

During the night when the air in contact with the ground is cooled, a nocturnal inversion is formed. When the sun rises in the morning, convection develops which tends to mix the air close to the ground, and thus creates a layer of constant potential temperature. There is entrainment of air into this mixed layer as the convection erodes away at the overlying inversion base. This process causes the inversion base to rise. General large-scale subsidence can partially or totally counteract this rise. Cooling of the air above the inversion base changes the inversion temperature lapse which in turn modifies the entrainment rate. The mixed layer is heated by the combined effects of an upward heat flux from the surface and a downward heat flux from the inversion layer. Prediction of these inversion-related characteristics, particularly the inversion height, are desirable for theoretical studies of the unstable boundary layer. It is with this incentive that the mathematical model of inversion rise presented in this paper was developed.

There have been numerous atmospheric observations and laboratory studies of these inversion characteristics. Izumi (1964), Kaimal (1966) and Lenschow and Johnson (1968) have observed inversions rising under the influence of surface convection, while Neiburger *et al.* (1961) and Mendonca and Iwaoka (1969) observed cases where subsidence was an additional influence. Laboratory studies have been conducted by Deardorff and Willis (1967), Turner (1968a,b) and Deardorff *et al.* (1969). These last two groups have photographed the overshoot and entrainment process occurring at the inversion interface. Penetrative convection has been observed in the atmosphere by Reynolds (1970) and Beran *et al.* (1971) using acoustic sounders.

Convection below the inversion base has been approached theoretically from two directions. One approach, as modeled by Priestley and Ball (1956), Morton *et al.* (1956), Baines and Turner (1969), Fox (1970, 1972) and Telford (1970, 1972) and as observed by Warner and Telford (1967), is that of looking at individual plumes. The other approach is that of describing the unstable boundary layer in terms of scaling velocities. This approach was taken by Tennekes (1970, 1971), Deardorff (1970a,b, 1972), Wyngaard *et al.* (1971), Businger (1972) and Arya (1972).

2. Approaches to the problem

Basically, two equations are needed to describe theoretically the height and temperature of the convective boundary layer. One is an equation describing the conservation of heat and the other expresses the conservation of mass under an entrainment assumption. If we formulate a relation, based on an assumed or idealized temperature structure in the inversion, that links entrainment rate to the downward heat flux at the inversion base, then we see that the desired entrainment assumption can be made either directly, or indirectly. Directly, an entrainment rate itself can be assumed. Indirectly, a downward heat flux can be assumed. Ball (1960) assumed a downward heat flux equal in magnitude to the surface heat flux, from consideration of the turbulent kinetic energy equation. Lilly (1968) recognized that such a heat flux assumption was unrealistically large, and so postulated that the magnitude of the actual downward heat flux lies between zero and that of Ball's assumption.

[1] Contribution No. 291, Department of the Atmospheric Sciences, University of Washington.

Alternately, by assuming that the convection is nonpenetrative, one arrives at the simple entrainment assumption that the rate of height change of the inversion base is equal to the rate of temperature change of the mixed layer divided by the initial lapse rate of the inversion [see review by Plate (1971)]. However, entrainment based on this assumption is smaller than that which is observed.

At the inversion base a physical process occurs which causes entrainment of air down into the mixed layer and which creates certain temperature and heat flux profiles. The entrainment assumptions described in the previous paragraphs are based on these observable effects of the physical process. However, the photographs published by Turner (1968b) and Deardorff *et al.* (1969) entice one to speculate on the actual physical process itself rather than on its effects. It will be this approach of describing the physical process itself to get an entrainment rate equation by which we will attempt in this paper to model the rise of inversions. Using this approach we will be able to predict a larger number of atmospheric variables than were predicted by the simpler models described above, necessitating a corresponding increase in the required number of equations. We will neglect the effects of latent heat and radiation.

3. Basic equations

From experiment we see that except for thin layers near the earth's surface and at the inversion base the mixed layer under an inversion, when averaged horizontally, is of constant potential temperature. If we neglect these thin layers, assume horizontal uniformity of the locally averaged means, and recognize that the rate of temperature change is approximately equal to the rate of potential temperature change, then the conservation of heat equation applied to the mixed layer is

$$F_0 - F_h = \rho C_p h(\partial\theta/\partial t), \tag{1}$$

where h is the present height of the base of the inversion, F_0 the surface turbulent heat flux, F_h the turbulent heat flux at h, ρ the density of air, C_p the specific heat at constant pressure of air, t time, and θ the horizontally and vertically averaged mean potential temperature of the mixed layer. Note that F_h is negative in the cases considered here, implying a downward turbulent heat flux at h. Also, by applying (1) to any height less than h, we see that the heat flux is a linear function of height. The potential temperature and heat flux profiles associated with an inversion under these approximations are shown in Fig. 1.

If we combine the simple entrainment assumptions as described earlier with (1), the resulting equation predicting the inversion height as a function of time is

$$h^2 - h_0^2 = \frac{2(F_0 - F_h)t}{\rho C_p \gamma'}, \tag{2}$$

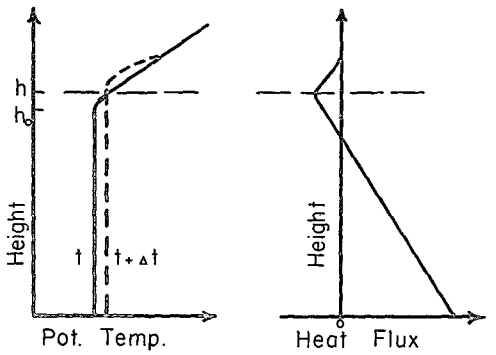

FIG. 1. Idealized profiles of potential temperature and turbulent heat flux associated with an inversion over penetrative convection.

where h_0 is the initial inversion base height and γ' the initial inversion potential temperature lapse rate. For simplicity, this initial lapse rate is assumed to be constant with height. Although (2) is not used in the present model, we see that if the present model is to always feel the effects of the initial lapse rate, then our present model should asymptotically predict a height-time dependence as shown by (2).

In the photographs referred to earlier, we notice that thermal convection, possibly in the form of plumes, tends to overshoot the inversion base to form protruding domes. These domes are visualized as sinking back into the mixed layer. While above the inversion base, there should be little entrainment between the fluid within the dome with the stable fluid outside of the dome. However, as a dome protrudes into the stable layer, "wisps" of fluid from above the inversion base may be visualized as being extruded between the plumes down into the mixed layer, in conformity with conservation of mass (see Fig. 2). These wisps would then be entrained into the mixed layer by the turbulent eddies present there, and thus not return above the inversion base.

The increase in mass due to entrainment of fluid into the mixed layer forces the inversion base to rise. This is counteracted to some extent by divergence associated with large-scale subsidence. The net change of height of

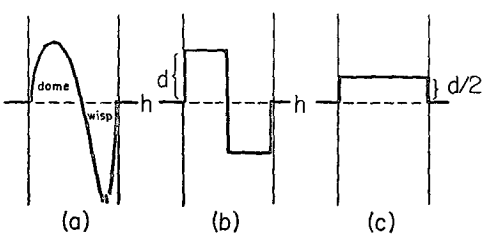

FIG. 2. Representation of penetrative convection. An idealized dome-wisp pair (a) can be pictorially represented by a square-shaped form (b), from which the resulting rise of the inversion base can be more easily seen (c) for the case of complete entrainment of the wisp.

the inversion base is thus

$$\frac{dh}{dt}=w_e+w_s(h), \tag{3}$$

where w_e is the entrainment velocity (rate of volume entrained per unit area) and $w_s(h)$ the synoptic-scale vertical velocity at h.

We put forth the following hypothesis to arrive at the entrainment velocity. On the average over a fixed area, there occurs a dome-wisp pair as shown in Fig. 2a, where h is defined such that the volume of the wisp equals the volume of the dome and where the average overshoot distance above the inversion base is d. By representing this dome-wisp pair by a square-shaped pair as shown in Fig. 2b, we can easily see that after the wisp is completely entrained, the inversion base in that area will have risen by $0.5d$, as in Fig. 2c.

With this definition of h as visualized in Fig. 2, we see that h is the level through which there is the maximum amount of eddy mass transfer caused by the domes and wisps. Assuming the fluid in the dome and in the wisp are each of uniform temperature throughout those separate features, then our definition of h is consistent with the usual definition used for h; that is, h is the level of maximum downward turbulent heat flux.

The entrainment velocity can now be defined as

$$w_e=\frac{\epsilon(0.5d)}{t_*}, \tag{4}$$

where t_* is a time scale reflecting how often a dome-wisp pair is formed. An entrainment coefficient ϵ has been included to take into account the fact that the wisp may not be completely entrained into the mixed layer, or similarly that some detrainment takes place in the stable region. The actual value for ϵ should be found from atmospheric measurements. The expressions needed to describe d and t_* are developed below.

The maximum overshoot distance d can be found by a force balance, yielding

$$d=\alpha w/\nu, \tag{5}$$

where w is the velocity of the plume as it just reaches the inversion base, and ν the Brunt-Väisällä frequency $(gT^{-1}\partial\theta/\partial z)^{\frac{1}{2}}$, and where the factor α takes into account the following counteracting plume properties which are not otherwise explicitly included in this derivation. One is that pressure forces in the vertical would tend to flatten the plume above the inversion base to become mushroom-like, thus forcing d to be smaller than idealized. However, the fact that the underlying plumes sustain the domes for a period of time longer than expected for a simple overshooting bubble would thus tend to increase d from that which is idealized. Since these effects tend to compensate each other, we would expect α to be approximately unity.

For simplicity, we will use $\partial\theta/\partial z\equiv\gamma$ where γ is the average potential temperature gradient over the distance of overshoot. If, on the other hand, the inversion can be characterized by a temperature discontinuity of $\Delta\theta$, then the maximum overshoot can be better represented by $d=w^2T/(2g\Delta\theta)$, where T is the mean temperature near the inversion base and g the acceleration due to gravity.

As referred to earlier, a scaling velocity has been derived which applies to the unstable boundary layer; this scaling velocity (w_*) is

$$w_*=\left(\frac{ghF_0}{T\rho C_p}\right)^{\frac{1}{3}}. \tag{6}$$

Deardorff's (1972) numerical results along with some experimental points included in his paper for comparison show that plume velocities as a function of relative height in the boundary layer can be scaled to (6). Assuming the rigid lid on Deardorff's model corresponds to the height of maximum overshoot in this hypothesis, and that the distance of plume overshoot is roughly 10% of the inversion height, then from Deardorff's Fig. 8 we see that

$$w\approx 0.4w_*. \tag{7}$$

This approximation is also in line with data from measurements by Telford and Warner (1964). This value for w can then be used in (5).

To find the entrainment rate, we must know how often a dome-wisp pair is formed. Assuming that plume velocities can be scaled to (6), and that plume heights are roughly equal to h, we see that convective plumes can be time-scaled by h/w_*. Since the dome-wisp pairs are formed from convective plumes, it is inviting to suggest that the frequency of occurrence of these pairs is related to this same scaling time. Based on acoustic sounding data taken by Reynolds (1970), we estimate the scaling time t_* for dome-wisp pairs to be

$$t_*\approx 0.35h/w_*. \tag{8}$$

This estimate is based on a number of cases where the mean wind was relatively weak, so that our estimate reflects the local generation rate of plumes rather than the advection of plumes past the sounder. This value for t_* can now be used in (4).

Combining (4), (5), (6), (7) and (8), we obtain

$$d=0.4\alpha\left(\frac{F_0}{\rho C_p}\right)^{\frac{1}{3}}\left(\frac{g}{T}\right)^{-\frac{1}{6}}h^{\frac{1}{2}}\gamma^{-\frac{1}{2}}, \tag{9}$$

$$w_e=0.57E\left(\frac{F_0}{\rho C_p}\right)^{\frac{2}{3}}\left(\frac{g}{T}\right)^{\frac{1}{3}}h^{-\frac{1}{3}}\gamma^{-\frac{1}{2}}, \tag{10}$$

where $E=\alpha\epsilon$.

To use (9) and (10) we must know how γ changes as the inversion rises. We can find this change in the follow-

ing manner. By assuming that the fluid in the wisp has come from the volume within $0.5d$ of the inversion base, and then assuming that the mean temperature of this fluid is the same as the fluid temperature in the middle of this layer (i.e., at $0.25Ed$), then we see that the heat flux at h is

$$F_h = -\rho C_p[\Theta|_{h+0.25Ed} - \theta]w_e, \tag{11}$$

where $\Theta(z)$ is the horizontally averaged, height-dependent potential temperature above the inversion base. Although in the real atmosphere not all of the plumes would overshoot to the same distance d, on the average (11) is valid.

The total cooling above the inversion base is

$$\frac{d\Theta(z)}{dt} = \frac{\partial\Theta(z)}{\partial t} + \mathbf{v}\cdot\nabla_h\Theta(z) + w_s\frac{\partial\Theta(z)}{\partial z} + \frac{\partial\overline{(w'\Theta')}}{\partial z}, \tag{12}$$

where $-\partial\overline{w'\Theta'}/\partial z$ is the cooling due to the turbulent overshoot of the plumes, $\mathbf{v}\cdot\nabla_h\Theta(z)$ is the horizontal advection of potential temperature in the small layer of interest, and $d\Theta(z)/dt$ indicates effects such as radiative cooling. Upon rearranging (12) and neglecting the effects of radiation and horizontal advection, we get

$$\frac{\partial\Theta(z)}{\partial t} = -w_s\frac{\partial\Theta(z)}{\partial z} - \frac{\partial\overline{(w'\Theta')}}{\partial z}, \quad \text{for } z>h. \tag{13}$$

This fact that not all of the plumes overshoot to the same distance, however, is important in determining the cooling distribution above the inversion base. By assuming a random variation of plume velocities at the inversion base, we would find a Gausian distribution of plume heights centered about d. Because the cooling rate associated with the overshoot of one plume is an asymmetric spike with maximum intensity at $d/2$, the cooling resulting from a Gaussian overshoot distribution would be a skewed bell-shaped curve with maximum intensity at $d/2$. For simplicity, however, it is convenient to assume that the cooling distribution itself is Gaussian. This can be expressed by

$$-\frac{\partial\overline{(w'\Theta')}}{\partial z} = \frac{4F_h}{(2\pi)^{\frac{1}{2}}\rho C_p d}\exp(-\tau^2/2), \quad \text{for } z>h, \tag{14}$$

where

$$\tau = [4(z-h)-2d]/d. \tag{15}$$

In (14) and (15) we have arbitrarily sized the Gaussian distribution such that about 95% of the cooling occurs within the distance d. We must remember that (14) and (15) are completely arbitrary; that is, if we know what the real distribution is, then we should use that in place of (14) and (15).

From integrating (13) over time, we see that we are finally able to describe the temperature profile above the inversion base. If we approximate this profile by

$$\gamma \approx \frac{\Theta|_{d+h} - \theta}{d}, \tag{16}$$

we now have the expression for γ that was needed for use in Eqs. (9) and (10). Combining this approximation for γ with (5) gives $d = w^2T/[g(\Theta|_{h+d} - \theta)]$, which we note is similar, within a factor of 2, to the expression for d for a finite temperature discontinuity of $\Delta\Theta$, as was written earlier.

Upon neglecting individual density change within the mixed layer, the continuity equation applied to the whole troposphere is

$$\frac{\partial w_s}{\partial z} = -\left(\frac{\partial u}{\partial x} + \frac{\partial v}{\partial y}\right), \tag{17}$$

where u, v, w_s are the wind velocities in the x (east), y (north) and z (upward) directions, respectively. If, for simplicity, we assume that the large-scale divergence as described by the right-hand side of (17) is equal to a constant b, then we see that the synoptic-scale vertical velocity is a linear function of height, i.e.,

$$w_s = -bz. \tag{18}$$

Our mathematical model of inversion rise is now completed. Eqs. (1), (3), (9), (10), (11), (13), (14), (15), (16) and (18) are a closed set with which we can predict h, θ, $\Theta(z)$, γ, w_s, w_e, d, F_h, $\overline{(w'\Theta')}$ and τ. Unfortunately, analytic solution of these nonlinear differential equations is difficult. The results of numerical solutions of the equations are presented in the next section.

The differential equations we have derived were approximated by finite-difference equations. These equations were then solved by starting with the given initial conditions and integrating with time increments of Δt. The calculation of values for the variables at time t were based on their old values at $t-\Delta t$. For example, in (16), the old values of $\Theta|_{d+h}$ and d at a time of $t-\Delta t$ were used to get a new γ for time t. Then this new γ was used in (5) to get a new value for d. Using this approach it is assumed that the time steps chosen will be small enough that the values of the variables do not change considerably during one time step. Numerical solution of these finite-difference equations was then performed with a time increment of 30–60 sec and a height increment above the inversion base of 1–3 m. These increment sizes were chosen to compromise between an accurately detailed solution and a solution with reasonable computer costs.

To get the initial value of d to use in the equations before the time steps were started, the following iterative scheme was used. First, an unrealistically large value of d was chosen. Then, finding the value of $\Theta|_{h+d}$

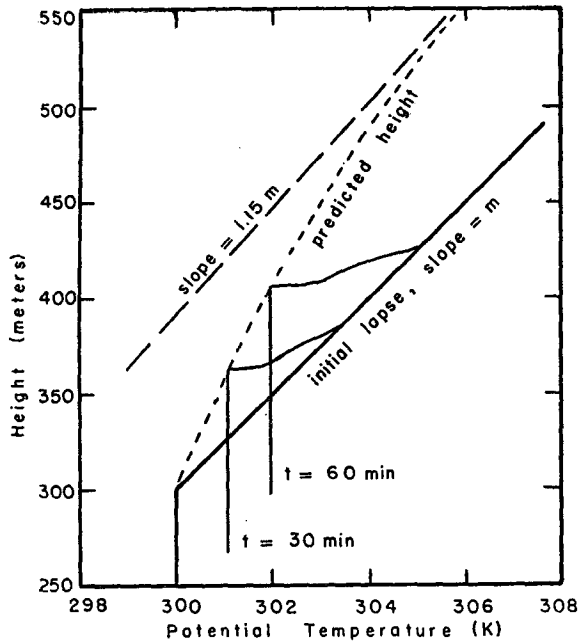

FIG. 3. Predicted inversion rise for the case of constant surface heat flux and no general subsidence.

using this initial guess for d and using the initial lapse rate, a new d was calculated. This procedure was repeated until d approached to within 1% of its asymptotic limit. It was this final value for d, and the associated value for $\Theta|_{h+d}$, that were used when the time steps were initiated.

4. Results

First, an examination of the equations is in order. From (3) and (10) we see that the boundary layer growth rate increases with increasing surface heat flux and decreases with increasing subsidence, lapse rate and inversion height. We also see that the heat flux at h cannot drive the whole system when there is no surface heat flux present (i.e., $F_h=0$ when $F_0=0$). The model was further examined through numerical solutions of the equations for a number of different cases.

For comparison purposes, the set of model equations were first solved with a constant surface heat flux of 20 mW cm^{-2} and with no subsidence. Finally, the surface heat flux was made a sinusoidal function of time to crudely simulate the daytime conditions, and subsidence was also included.

In the case of constant heat flux, an initial inversion lapse rate of 0.04K m^{-1} was used with an entrainment coefficient arbitrarily chosen to be 1.0. The rise of the inversion is shown in Fig. 3. We see that the inversion height as a function of temperature is greater than that predicted by the initial lapse rate. This fact is observed in the atmosphere. Although there is a change in lapse rate immediately above the inversion base as is seen in nature, there is also a finite temperature step at h which is not found in nature. This unrealistic step would not have been present if we had included the effects of turbulence which is induced in the stable layer. Such turbulence would smooth out the temperature profiles above h.

At $t=60$ min in Fig. 3, for example, we see the distance d of plume overshoot is indicated by that region above the inversion base where the temperature has cooled to below that of the initial lapse. Although a temperature step has been generated by the model in part of this region, we see that the whole region within distance d of the inversion base is best represented by a lapse rate approximated by (16) rather than by a temperature step of $\Delta\Theta$. This is the justification for the use of (16) and (5).

We can also see that the steepening of the lapse just above the inversion base causes the entrainment rate w_e to decrease. As is shown in Fig. 3, the inversion height asymptotically approaches a line of slope 1.15 times the slope of the initial lapse. We see from (1) that this is expected if the heat flux at h asymptotically approaches $-0.15F_0$, which is indeed what was found. Furthermore, this general asymptotic limit for the constant surface heat flux case agrees with what has been found in the planetary boundary layer.

If the effects of the initial lapse are continuously felt by the rising inversion, then we should expect the inversion height to approach a height-time functional relationship similar to that predicted by (2). The fact that this relationship was indeed found (as is shown in Fig. 4) gives evidence that the lapse rate above the inversion base, rather than the temperature step, was the controlling influence.

Another case was tried in which subsidence was assumed to be a linear function of height, and surface heat flux was sinusoidal. The parameters were chosen to coincide with those present in the fifth general observation period of the Great Plains experiment (Lettau and Davidson, 1957) as a test to see if this model can represent what was actually observed.

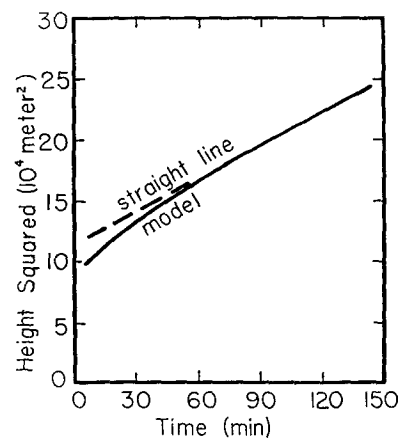

FIG. 4. Asymptotic dependence of the square of the predicted inversion height upon time.

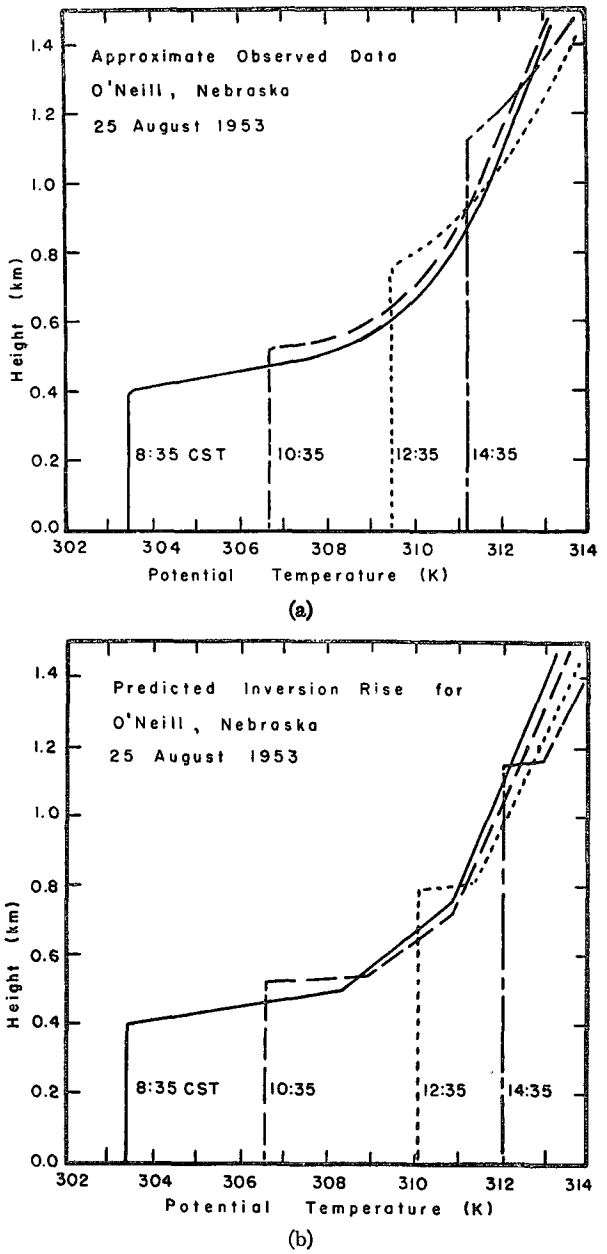

FIG. 5. Comparison of the model predictions (b) with approximate observed data of the Great Plains Experiment (a), where the initial lapse as indicated by the solid line in (a) has been approximated by the three solid straight line segments in (b).

The approximate initial lapse present in the data as shown by the solid line in Fig. 5a was approximated by the three straight solid lines in Fig. 5b. Based on the observed drop of an upper level inversion during the course of the day, the divergence was chosen to be $b=9.23\times10^{-6}$ sec^{-1}. The initial potential temperature and height of the mixed layer used in the model were 303.4K and 404.6 m, respectively. Again, the entrainment coefficient was arbitrarily set to 1.0. A sinusoidal function with half-period of about 9 hr and maximum amplitude of 33 mW cm^{-2} was used to describe the surface heat flux.

The results are shown in Figs. 5a and 5b, where 5a shows the approximate observed data and 5b the computed data. We see that the inversion height was computed very accurately, while the temperatures were off by about 0.8K by the end of the day. This error is in part due to the imprecise heat flux, radiation, and subsidence input forcings. We also see that the model does not predict enough cooling above the inversion base. This imperfection is also believed to be caused by the fact that effects such as radiation and advection were not included in this model. We did note, however, that the results predicted by this model are relatively insensitive to the value of E.

By measuring the actual downward turbulent heat flux at h, we should be able to calculate the corresponding value of E. As an example of F_h as a function of E and time, the sinusoidally varying surface heat flux conditions as modeled for the Great Plains data are used to generate the information shown in Fig. 6. Thus, if F_h could have been determined from the actual Great Plains data, then we could refer back to Fig. 6 to get E.

As described earlier, ϵ is defined in the idealized model to be a measure of the percentage of the wisp that is entrained into the mixed layer. However, when calculating ϵ from actual observed values of F_h, we now should consider the influences of other processes in the real atmosphere which we have neglected in our

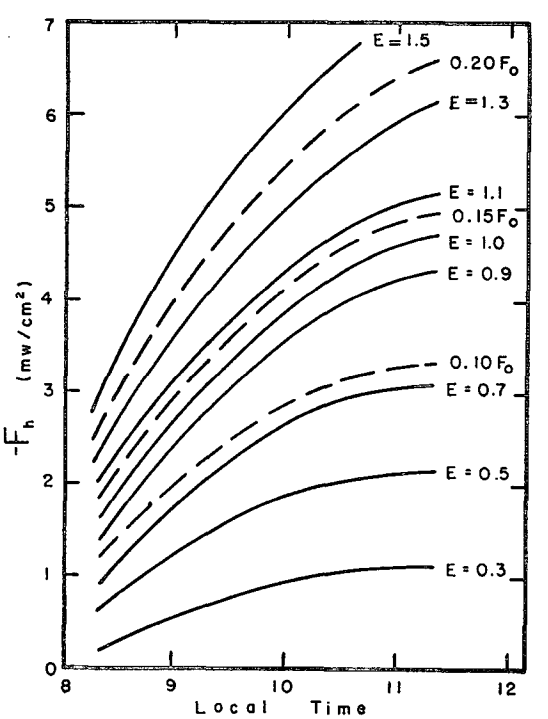

FIG. 6. Relationship between the downward heat flux at the inversion base and the entrainment coefficient for a sinusoidally increasing surface heat flux.

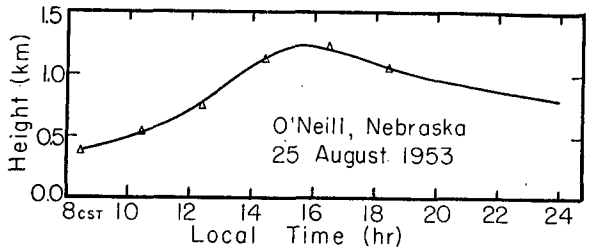

FIG. 7. Predicted inversion height (solid line) during the course of a day. This predicted height agrees very closely with the actual observed height (data points) for which it was modeled.

idealized model. For example, detrainment of air from the protruding domes upward into the stable layer above the inversion base can affect the value of ϵ. Also, for a rapidly changing surface heat flux, the measured value of F_h at any instant may not be in equilibrium with the value of F_0 at that instant. Thus, we see that ϵ no longer has the pure definition used earlier for the idealized model.

In general, we do see that the model realistically predicts the inversion rise in the morning and early afternoon, and its fall in late afternoon as the entrainment rate becomes weaker than the subsidence. Finally, at night, the entrainment ceases entirely letting subsidence push the inversion base (defined now by the passive temperature lapse rate rather than the dynamic level of maximum downward heat flux) downward. Such a time profile prediction is presented in Fig. 7, where this profile agrees very closely with the actual Great Plains data.

5. Conclusions

The equations we have used in modeling the characteristics associated with inversion rise are (1), (3), (9), (10), (11), (13), (14), (15), (16) and (18). We have seen that these equations simulate many of the properties of inversions, and may be used with a fair degree of accuracy in predicting real inversion rises in the atmosphere.

We must remember, however, the limitations of this model. By assuming well-organized free convection, we see that the model is not applicable to the initial rise of a nocturnal inversion where, within a few Obukhov lengths of the surface, wind shear is important. During the night in situations where convection ceases, we recognize that subsidence is the controlling influence, pushing the inversion toward the surface.

We also must remember that the numerical coefficients used in (7) and (8) are crude estimates based on very limited data; further experiments are planned to determine these coefficients more accurately. However, within its limitations, it is hoped that this model will be helpful for use with general models of the unstable boundary layer.

The relative success of this model in describing inversion characteristics sparks interest in making further refinements and extensions. We plan to incorporate the effects of radiation and advection into the model. Also, we plan to include wind shear effects to extend the range of applicability of the model to cases where the inversion is near the earth's surface. The effects of a combined lapse rate and temperature step above the inversion base will also be included by generalizing (5) to include a temperature step. Eventually, we hope to include atmospheric situations where clouds are present by looking at latent heat changes.

Acknowledgments. The support, encouragement, and helpful suggestions offered by Joost Businger during the development of this model are gratefully acknowledged. I also wish to thank James Deardorff for reviewing this paper and offering helpful comments. Research on this model was supported by the National Science Foundation under Grant GA 31317X1.

REFERENCES

Arya, S. P. S., 1972: Free convection similarity and measurements in flows with and without shear. *J. Atmos. Sci.*, **29**, 877–885.

Baines, W. D., and J. S. Turner, 1969: Turbulent buoyant convection from a source in a confined region. *J. Fluid Mech.*, **37**, 51–80.

Ball, F. K., 1960: Control of inversion height by surface heating. *Quart. J. Roy. Meteor. Soc.*, **86**, 983–994.

Beran, D. W., C. G. Little and B. C. Willmarth, 1971: Acoustic Doppler measurements of vertical velocities in the atmosphere. *Nature*, **230**, 160–162.

Businger, J. A., 1971: Comments on "Free convection in the turbulent Ekman layer of the Atmosphere." *J. Atmos. Sci.*, **28**, 198–299.

——, 1972: The atmospheric boundary layer. *Remote Sensing of the Troposphere*, V. E. Derr, Ed., NOAA, Washington D. C., Chap. 6.

Deardorff, J. W., 1970a: Preliminary results from numerical integrations of the unstable planetary boundary layer. *J. Atmos. Sci.*, **27**, 1209–1211.

——, 1970b: Convective velocity and temperature scales for the unstable planetary boundary layer and for Rayleigh convection. *J. Atmos. Sci.*, **27**, 1211–1213.

——, 1972: Numerical investigation of neutral and unstable planetary boundary layers. *J. Atmos. Sci.*, **29**, 91–115.

——, and G. E. Willis, 1967: Investigation of turbulent thermal convection between horizontal plates. *J. Fluid Mech.*, **28**, 675–704.

——, —— and D. K. Lilly, 1969: Laboratory investigation of nonsteady penetrative convection. *J. Fluid Mech.*, **35**, 7–31.

Fox, D. G., 1970: Forced plume in stratified fluid. *J. Geophys. Res.*, **33**, 6818–6835.

——, 1972: Numerical simulation of three-dimensional shape-preserving convective elements. *J. Atmos. Sci.*, **29**, 322–341.

Izumi, I., 1964: The evolution of temperature and velocity profiles during breakdown of a nocturnal inversion and a low-level jet. *J. Appl. Meteor.*, **3**, 70–82.

Kaimal, J. C., 1966: An analysis of sonic anemometer measurements from the Cedar Hill tower. AFCRL-66-542, Environ. Res. Paper 215.

Lenschow, D. H., and W. B. Johnson, Jr., 1968: Concurrent airplane and balloon measurements of atmospheric boundary-layer structure over a forest. *J. Appl. Meteor.*, **7**, 79–89.

Lettau, H. H., and B. Davidson, 1957: *Exploring the Atmosphere's First Mile*, Vol. 2. New York, Pergamon Press, 578 pp.

Lilly, D. K., 1968: Models of cloud-topped mixed layers under a strong inversion. *Quart. J. Roy. Meteor. Soc.*, **94**, 292–309.

Mendonca, B. G., and W. T. Iwaoka, 1969: The trade wind inversion at the slopes of Mauna Loa, Hawaii. *J. Appl. Meteor.*, **8**, 213–217.

Morton, B. R., G. I. Taylor and J. S. Turner, 1956: Turbulent gravitational convection from maintained and instantaneous sources. *Proc. Roy. Soc. London*, **A234**, 1–23.

Musman, S., 1968: Penetrative convection. *J. Fluid Mech.*, **31**, 343–360.

Neiburger, M., D. S. Johnson and C. Chien, 1961: Studies of the structure of the atmosphere over the Eastern Pacific Ocean in summer—1. The inversion over the Eastern North Pacific Ocean. *Univ. Calif. Publ. Meteor.*, **1**, No. 1, 1–58.

Plate, E. J., 1971: *Aerodynamic Characteristics of Atmospheric Boundary Layers*. U. S. Atomic Energy Commission Critical Review Series, Natl. Tech. Inform. Serv., Dept. of Commerce, 121–133.

Priestley, C. H. B., and F. K. Ball, 1956: Continuous convection from an isolated source of heat. *Quart. J. Roy. Meteor. Soc.*, **81**, 144–157.

Reynolds, R. M., 1970: An acoustic radar for studying low-level atmospheric phenomenon. M.S. thesis, University of Melbourne, Australia.

Telford, J. W., 1970: Convective plumes in a convective field. *J. Atmos. Sci.*, **27**, 347–358.

——, 1972: A plume theory for the convective field in clear air. *J. Atmos. Sci.*, **29**, 128–134.

——, and J. Warner, 1964: Fluxes of heat and vapor in the lower atmosphere derived from aircraft observations. *J. Atmos. Sci.*, **21**, 539–548.

Tennekes, H., 1970: Free convection in the turbulent Ekman layer of the atmosphere. *J. Atmos. Sci.*, **27**, 1027–1034.

——, 1971: Reply. *J. Atmos. Sci.*, **28**, 300–301.

Turner, J. S., 1968a: The behavior of a stable salinity gradient heated from below. *J. Fluid Mech.*, **33**, 183–200.

——, 1968b: The influence of molecular diffusivity on turbulent entrainment across a density interface. *J. Fluid Mech.*, **33**, 639–656.

Warner, J., and J. W. Telford, 1967: Convection below cloud base. *J. Atmos. Sci.*, **24**, 374–382.

Wyngaard, J. C., O. R. Coté and Y. Izumi, 1971: Local free convection, similarity, and the budgets of shear stress and heat flux. *J. Atmos. Sci.*, **28**, 1171–1182.